Diyala Journal of Engineering Sciences

Journal homepage: https://djes.info/index.php/djes

ISSN: 1999-8716 (Print); 2616-6909 (Online)

Thermodynamic and Exergetic Analysis of an LNG-Assisted CCHP Plant with LiBr/Water ARC

Saadoon Abdul Hafedh[1], Layth Abed Hasnawi Al-Rubaye[1*], Faramarz Ranjbar[2], Moharram Jafari[2]

[1] Department of Mechanical Engineering, College of Engineering, University of Diyala, Baquba, Diyala Province, Iraq.
[2] Department of Mechanical Engineering, University of Tabriz, Tabriz, Iran.

ARTICLE INFO

Article history:
Received: 27/05/2025.
Revised: 23/10/2025.
Accepted: 04/11/2025.
Available online: 10/12/2025

Keywords:
LNG regasification
Cold energy recovery
CCHP
Waste heat recovery
Absorption refrigeration (LiBr/Water ARC)

ABSTRACT

This study proposes a novel liquefied-natural-gas-assisted combined cooling, heating, and power (CCHP) plant in which the cryogenic energy released during regasification is cascaded through a closed nitrogen Brayton cold-box, medium-temperature heat is coupled to a toluene organic Rankine cycle (ORC), and a lithium-bromide/water absorption refrigeration cycle (ARC) provides cooling while domestic hot water at 60 °C is recovered. A comprehensive steady-state model was developed in Engineering Equation Solver (EES) and benchmarked against three published data sets; the largest deviations were 2.8% for the gas-turbine block and 0.3% for the chiller, confirming the model's reliability. Energy and exergy balances were solved simultaneously for every component, enabling consistent comparison of power-only, CHP, and CCHP modes for a 160-MW-class plant. Under nominal conditions the system delivers 168.8 MW net power, 11.7 MW cooling, and 143.7 kg/s hot water, with energy and exergy efficiencies of 93.2% and 51%, respectively. Parametric sweeps of combustor outlet temperature, compressor pressure ratio, LNG regasification pressure, and heat exchanger pinch points expose design trade-offs, pinpoint a practical 6–7 MPa regasification-pressure window, and versus a recent benchmark lift exergy efficiency from 41% to 51% (~24% gain) while cutting specific fuel consumption by 18% at equal net power. These improvements are achieved without exotic working fluids or deep cryogenic stages, making the concept deployable with current hardware. The integrated methodology and data set form a transferable benchmark for future LNG-based energy hubs and highlight clear upgrade paths most notably staged combustion and advanced heat-exchanger networks to push performance even further.

1. INTRODUCTION

The increasing global consumption of liquefied natural gas (LNG) reflects a shift towards cleaner energy sources, positioning it as a pivotal player in the energy landscape. The regasification process, which transitions LNG from cryogenic states to usable forms, holds considerable promise for energy recovery. This phase inherently possesses a substantial amount of cold energy that, if harnessed properly, could enhance sustainable power generation and boost the efficiency of LNG regasification facilities. Nonetheless, the potential for recovering and utilizing this cold energy remains largely untapped, especially when considering the integration of advanced thermodynamic cycles for power generation [1–4]. Recent studies have revealed noteworthy progress in the fusion of thermodynamic cycles with LNG cold energy recovery for the purpose of power generation.

For instance, Cao et al. [5] introduced a biomass-fueled triple combined cycle and This system is thermionically optimized by integrating with LNG regasification to utilize its cold exergy for cooling the compressor inlet. The refined system delivered a total power output of 8578 kW, which includes 5656 kW generated by the gas turbine, 1194 kW from the CBC,

*Corresponding author's Email address: laythabed2014@gmail.com
DOI: 10.24237/djes.2025.18412

777.4 kW from the ORC, and 745.3 kW from the LNG loop. The system achieved an exergy efficiency of 41.01%.

Similarly, a biogas-fed hybrid trigeneration system, LNG cold energy recovery, absorption refrigeration, and a proton exchange membrane electrolyzer (PEME) to achieve simultaneous production of power, cooling, and hydrogen presented by Khanmohammadi et al. [6]. The reported net output power is 39.9 MW. Additionally, the refrigeration system adds 473.52 kW, culminating in a total plant yield of 7.265 kg/h of H_2. The refined setup realizes an energy efficiency of 50.69% and an exergy destruction rate of 42590.74 kW.

Yousef et al. [7] presented a sustainable multigeneration system using an ammonia-water absorption refrigeration cycle to generate electricity, cooling, heating, and hydrogen. Simulations show a net power output of 259.184 MW, cooling and heating capacity of 88.938 MW and 2.839 MW, and hydrogen generation of 391.68 kg/h. The suggested system has energy and exergy efficiencies of 62.79% and 54.90%, respectively, and a low product cost of 11.35 $/GJ, making it a promising clean energy alternative.

Tsatsaronis and Morosuk. [8] conducted an advanced exergetic analysis of a novel co-generation system that combines LNG regasification with electricity generation, aiming to improve the efficiency of LNG regasification processes. Yehia et al. [9] suggested a comprehensive energy system that integrates a single-effect mixed refrigerant cycle, liquefied air energy storage, and LNG regasification to enhance the efficiency of cold energy use and electricity production.

Xu et al. [10] introduced a groundbreaking polygonation system that merges biomass combustion with LNG regasification, aiming to provide a comprehensive solution for CCHP, and freshwater. Their goal is achieved through thermally integrated subsystems, which include an ORC, multi-effect desalination (MED), and an absorption chiller.

Zhao et al. [11] introduced a framework for cascade heat integration that merges a gas turbine cycle with LNG cold energy regasification for multigeneration purposes, encompassing electricity, heating, cooling, and freshwater production. the system showed high energy efficiency of 92.92% and exergy efficiency of 63.5%, producing a net power output of 22,977 kW, along with 4650.5 kW of cooling, 18,561 kW of heating, and freshwater, all with a heat input of 302.3 kW.

Liu et al. [12] investigated a cool clean efficient power system (COOLCEP-S), a zero CO_2-emission, high-efficiency power and refrigeration cycle that utilizes LNG coldness. Through optimization, they achieved an energy efficiency of 59% at a turbine inlet temperature of 900°C. Liang et al. [13] developed a biogas-based polygonation system that incorporates LNG cold exergy-driven cryogenic separation for biogas upgrading, alongside a Kalina cycle, ORC, MED, and a heating unit, enabling the simultaneous production of power, hot water, fresh water, and liquid CO_2.

Salehi and Javanfam [14] proposed a solar-assisted multigeneration system with two ORCs, an absorption refrigeration (AR) unit, a single-effect absorption heat transformer (AHT), and three water desalination systems closed and open HDH and an evaporative unit. Simulations in Ahvaz, Iran, generated 21.46 kW of power, 71.02 kW of refrigeration, and 100.65 g/s of distilled water.

The multi-generation system by Emadi and Mahmoudimehr [15] uses geothermal heat and LNG regasification as the heat sink. This system uses two ORCs, an ARC, and a PEM electrolyzer to create electricity, heating, cooling, and hydrogen. A GA-ANN hybrid model optimizes costs and efficiency. The optimized system produced 7.92 MW of net electricity, 14.47 MW of cooling, and 10.48 MW of heating. It also claimed $1.738/kg levelized hydrogen and 1.505 cents/kWh power costs.

An LNG cold energy heat sinks improved thermal performance and sustainability in a biomass-fueled multigeneration energy system including a gasifier-gas turbine cycle, Rankine cycle, cascade ORC, ARC, and PEM electrolyzer by Taheri et al. [16].

Cooling load was 2355 kW, net electricity generation 25,164 kW. Hydrogen generation produced 39.2% energy and 25.7% exergy efficiency using 6411 kW of power. Optimization indicated that increasing turbine intake temperature to 1230°C boosted exergy efficiency by 29.4% and decreased cost by 3.2%.

Hu et al. [17] created power, cooling, and hydrogen from a gas turbine using a steam Rankine cycle (SRC), two organic ORCs, an absorption refrigeration unit, a PEM electrolyzer, and LNG regasification. The system produced 78.76 MW of net power, comprising 55.84 MW from the gas turbine, 11.39 MW from the SRC, 7.48 MW from ORCs, 4.05 MW from LNG, and 185.15 kg/h of hydrogen, in normal operation.

Hamada et al. [18] modeled a 750 MW combined-cycle power plant (Tuanku Ja'afar, Malaysia) and, after validation with plant data, reported 56% energy and 51% exergy efficiencies; the gas-turbine combustion chamber dominated irreversibility (224.6 MW, 67.5% of total), TIT > 1262 °C reduced combustor exergy destruction, and closing the diverter to the HRSG lifted plant thermal efficiency to 55% with about 260 MW added by the steam cycle (vs 34–35% in simple-cycle operation).

Mohammed et al. [19] analyzed a 200 MW Shahid Montazeri steam plant and showed that increasing feedwater heaters (FWHs) to nine raised efficiencies to 37.52% (energy) and 41.7% (exergy), identified the boiler/combustor as the main exergy-destruction site (48% of fuel exergy), and indicated an optimal reheat pressure 20–25% of boiler pressure; at 160 bar boiler pressure, adding the initial FWH increased exergy efficiency from 34% to 37%.

Current LNG-assisted combined cooling, heating, and power (CCHP) studies typically examine only one or two subsystems in isolation—for example, reclaiming cryogenic exergy to chill inlet air, or pairing a gas-turbine combined cycle with a lithium-bromide chiller. What is still missing is an integrated thermodynamic framework that tracks energy and exergy through all major streams when an LNG regasification line, a closed Brayton cold box, a conventional combined cycle, and an absorption refrigeration cycle are tightly coupled. Likewise, most published parametric studies treat the LNG stream as a fixed "cold sink," leaving unanswered questions about how regasification pressure, mass-flow allocation, or heat-exchanger pinch points influence the overall plant and each utility product (power, chilled water, process heat). Without that system-wide perspective, designers lack clear guidance on where irreversibilities concentrate or how to priorities hardware upgrades.

1.1 Novelty and Contributions:

This work fills the gap by proposing and rigorously modelling a fully integrated LNG-assisted combined cooling, heating, and power (CCHP) plant under a unified energetic exergetic framework. The cold energy released during regasification is cascaded through a closed nitrogen Brayton loop and subsequently coupled to a LiBr/H_2O absorption chiller, while medium-temperature heat from an open Brayton combustor branch drives a toluene organic Rankine cycle and supports domestic hot water production.

A single, validated Engineering Equation Solver (EES) implementation captures mass, energy, and exergy balances for every component, enabling consistent comparison of power-only, CHP, and CCHP operating modes and systematic exploration of key design variables.

In contrast to previous LNG integrations that primarily target power augmentation (LNG-Rankine/ORC) or partial co-generation without full tri-generation and without unified exergy accounting across all subsystems, the present end-to-end architecture co-integrates CBC+OBC+ORC+ARC with explicit pinch and pressure-drop constraints and intercooling.

Within this holistic treatment, we demonstrate full tri-generation (electricity, space cooling, and domestic hot water) with a system-level exergetic efficiency of approximately 51%, identify a practical regasification-pressure window that maximizes overall performance via parametric mapping, and provide a component-resolved exergy-destruction breakdown that isolates the dominant irreversibilities (combustion chamber and heat-exchange network), thereby guiding design trade-offs. These elements collectively clarify the interplay among the sub-cycles, extend beyond prior LNG cold-energy schemes, and establish a transferable methodology for evaluating future LNG-assisted poly-generation across different plant sizes and duty splits. A comparative summary against recent studies is provided in Table 1.

Table 1: Focused comparison with representative LNG-integration studies

Study	System boundary & coupling	Products considered	Key analyses reported	Gaps vs. this work
Cao et al. [5]	LNG cold-energy recovery with power-oriented coupling (per your citation)	Power / Cooling (as reported)	Energy/exergy; cycle-level assessment	No full CCHP with DHW; no unified CBC+OBC+ORC+ARC co-integration; no Regas pressure window mapping
Zhao et al. [11]	LNG-related integration with performance optimization (per your citation)	Power ± Cooling (as reported)	Energy/exergy; optimization	Not tri-generation; lacks component-wise exergy-destruction map across all subsystems
Emadi & Mahmoudimehr. [15]	Modelling & thermoeconomics using LNG as heat sink	Power / Cooling (as reported)	Energy/exergy + thermos-economics	No DHW; not a single polygonation framework; no unified energy–exergy basis over CBC+OBC+ORC+ARC
Taheri et al. [16]	LNG regasification integrated with H_2	Power / Hydrogen	Energy/exergy/eco-nomic	Not CCHP; ARC not co-integrated; no cryogenic

	production (different target)			CBC cold-box exploitation
Hamada et al. [18]	Conventional CCPP (no LNG cold-recovery); validated against plant data	Power	Plant-wide energy/exergy; component-wise exergy destruction; TIT parametric	No LNG cold-energy utilization; no tri-generation; no unified CBC + OBC + ORC + ARC; no Regas pressure window.
This work	CBC (N_2) + OBC + ORC (toluene) + LiBr–H_2O ARC under unified energy–exergy framework with pinch/Δp constraints and intercooling	CCHP: Power, Space Cooling, DHW	Energy/exergy; unified CCHP-level performance assessment; regasification-pressure window; component-wise exergy-destruction mapping	Modelling a fully integrated LNG-assisted combined cooling, heating, and power (CCHP) plant under a unified energetic exergetic framework

2. METHODOLOGY

2.1 System layout description

Figure 1 presents a detailed diagram describing a sequential process intended for harvesting cold energy from low-temperature LNG via a series of thermodynamic cycles. The cold LNG in its initial state at cryogenic temperature and moderate pressure is subjected to compression, resulting in a higher pressure (State 2). This acts as the main source of cold energy for the whole system. From this position, the LNG transitions to a heat exchanger (HEX 1), so it starts to absorb the heat from the N2 while preserving its elevated pressure with a minimal pressure drop of 1% (States 2-3). Upon receiving heat, the fluid undergoes expansion through the primary turbine (NGT 1) and is subsequently conveyed to the industrial facility (State 4).

A small percentage of the methane stream is redirected, reheated utilizing waste heat in HEX 3, and expanded through a medium-pressure turbine (NGT 2). This procedure elevates its temperature and optimizes its pressure for the Combustion Chamber (C.C.) that is installed in the OBC section (State 18,19,13). The CBC cycle behaves as the middle cycle, commencing at the point where the N2, under low temperature and pressure, exits HEX 1 after extracting cold energy from the LNG cycle (State 5). Subsequently, the working fluid is directed to N2 compressor, where an increase in pressure is achieved through a compression process (State 6). The high-pressure N2 gets its thermal energy from the flue gases and, after exiting, flows to N2 turbine, where it expands to a lower pressure before returning to State 5 to complete the closed cycle (States 7-8).

The OBC subsystem engages as the ambient fresh air undergoes initial compression in a compressor (AC 1), elevating its pressure (State 9). Subsequently, it undergoes cooling in the HEX 4 and Generator, where leftovers thermal energy is transferred to the ORC's working fluid and LiBr/water subsystem (state 11, 12). Following this, air is further compressed in the compressor (AC 2) and then routed to the Combustion Chamber (CC), where it collaborates in combustion with LNG-derived methane through NGT 2, resulting in the generation of high-temperature combustion gases (States 20,14). The combustion gases undergo expansion in the expander (GT) prior to being systematically cooled in heat exchangers (HEXs 2 and 3), finally being released into the atmosphere (States 15-17). The ORC cycle utilizes Toluene as its working fluid, initiating the process by absorbing heat from HEX 4 and subsequently flowing to the ORC Turbine, where it undergoes a pressure reduction through an expansion process.

The low-pressure fluid conveys its thermal energy to the HEX 5 -that use for producing DHW mass flow rate- and upon exiting, it moves to ORC pump, where it gets a higher pressure before making its way back to HEX 4 to finalize the ORC (States 23-24). Eventually, within the absorption refrigeration cycle, the weak LiBr/water fluid is separated into two different streams: dense LiBr/water and water vapor, which serves as the refrigerant. This process occurs as heat is absorbed from the generator, which is powered by the air cycle (points 29, 30, 34). Upon exiting the condenser, the stream of water vapor approaches a Expansion valve, prepared to absorb heat within the designated evaporator of the system. The saturated vapor that leaves the evaporator subsequently makes its way into the absorber (points 31, 32, and 33).

The dense flow generated in the system proceeds to a Expansion valve following it's journey through the intermediate HEX 6, aiming to achieve the desired absorber pressure at points 35 and 36. Subsequently, it merges with the saturated vapor stream from the evaporator within the absorber, finally exiting as a weak stream (point 27). Upon navigation this single pump within the absorption refrigeration cycle, it

reaches the generator pressure and then proceeds into the generator after acquiring heat in the HEX 6.

2.2 System modelling and thermodynamic analysis

First- and second-law analyses were applied to the enhanced combined cooling, heating, and power (CCHP) system. The process modelling and simulations adopt the following assumptions:

- The plant operates at steady state and steady flow conditions.
- External heat-transfer losses to the environment are neglected, except for a representative 2% casing loss applied to the combustion chamber (Table 2).
- Changes in kinetic and potential energy are neglected.
- Pressure drops within pipes and equipment are included, as specified in Table 2.
- Thermal approach constraints are enforced as follows: CETD = 15 °C on the ORC side; HEX-6 effectiveness = 85% in the ARC; and the air-side intercooler approach is maintained within a typical design band of ≥ 5–10 K, consistent with the reported state temperatures.
- Auxiliary powers (LNG pump, CBC compressors/expanders, ORC pump, ARC solution pump) are accounted for in the plant balances and thus reflected in W_{net}.

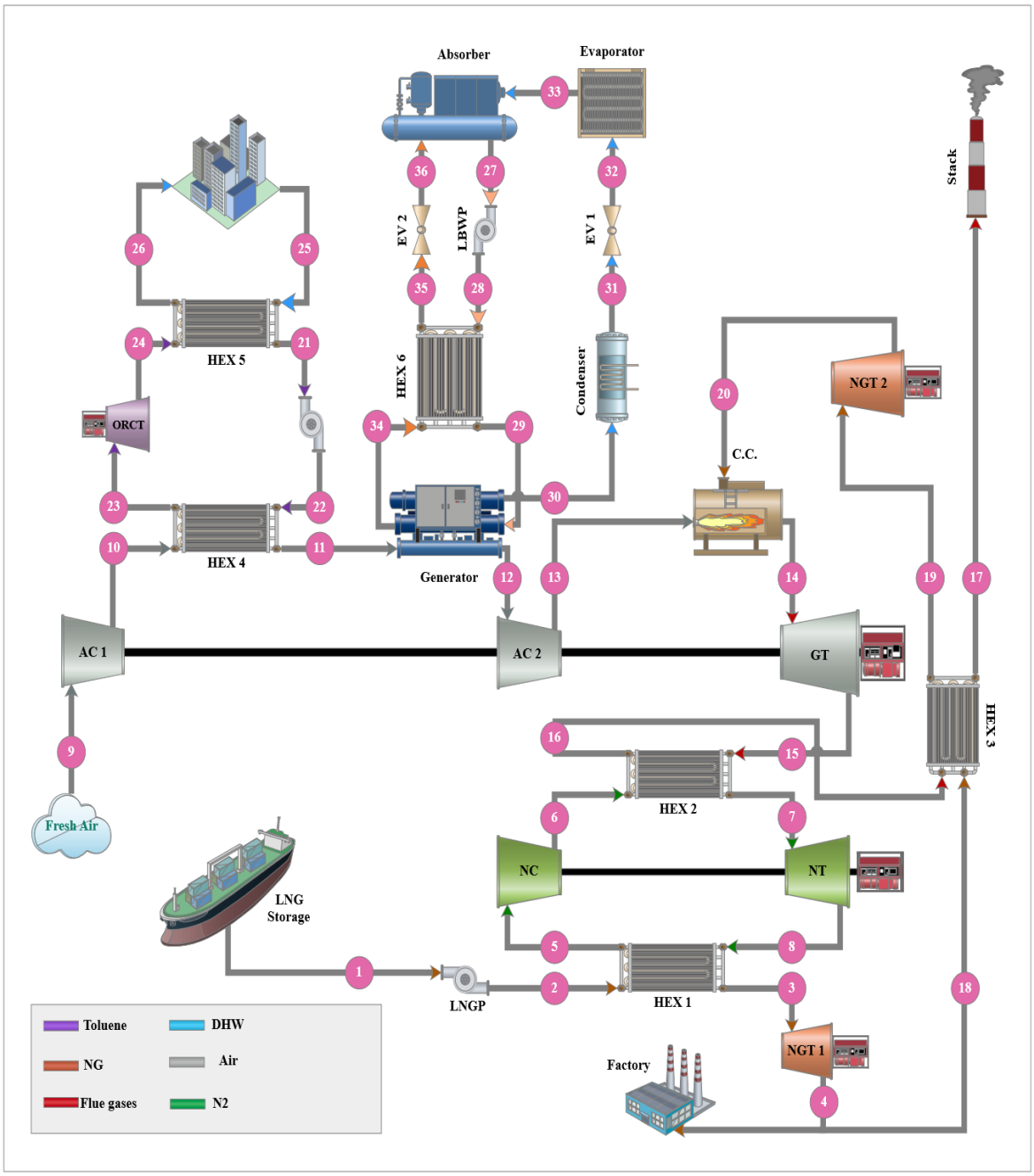

Figure 1. Configuration of the proposed CCHP system.

2.3 Data set-up and governing equations

Table 2 shows the input parameters used in the simulation of the proposed CCHP system.

The power facility is fundamentally composed of heat exchangers, turbines, compressors, expanders, pumps, and a CC, reflecting a complex interplay of components essential for its operation. In alignment with the foundational tenets of mass and energy conservation articulated in the first law of thermodynamics, a thorough establishment of mass and energy balances is undertaken to assess the operational efficiency of the power plant. The principles of mass conservation and energy balance for a control volume functioning under steady-state conditions can be expressed in the way that follows [20]:

$$\sum_{inlets} \dot{m}_i = \sum_{outlets} \dot{m}_e \quad (1)$$

$$\dot{Q}_{cv} - \dot{W}_{cv} = \sum_{inlets} \dot{m}_i h_i - \sum_{outlets} \dot{m}_e h_e \quad (2)$$

$$\dot{W}_{net} = \sum \dot{W}_T - \sum \dot{W}_C - \sum \dot{W}_P \quad (3)$$

Net heat input of each cycle:

$$\dot{Q}_{in} = \dot{m}(h_i - h_e) \quad (4)$$

Table 2. CCHP system input parameters data

Parameter	Value	Unit
Reference State		
Pressure (P_0)	101.3	kPa
Temperature (T_0)	15	℃
LNG		
Storage Pressure	10000	kPa
Storage Temperature	-162	℃
Pump isentropic efficiency	66.5	%
Turbine isentropic efficiency	85	%
CBC (N2)		
Compressor isentropic efficiency	85	%
Turbine isentropic efficiency	88	%
Pressure ratio	15	-
OBC (Air)		
Air pressure	101.3	kPa
Air temperature	181	℃
Combustion temperature	1290	℃
Air compressors isentropic efficiency	90	%
Turbine isentropic efficiency	94	%
Combustion chamber heat loss	2	%
Air compressors pressure ratio	42	-
ORC (Toluene)		
Evaporator Temperature	150	℃
Condenser Temperature	40	℃
Turbine isentropic efficiency	90	%
Pump isentropic efficiency	88	%
Cold End Temperature Difference (CETD)	15	℃
LiBr/Water Cycle		
Generator dense solution outlet Temperature	100	℃
Absorber solution outlet Temperature	30	℃
Condenser water outlet temperature	30	℃
Evaporator Temperature	5	℃
Cold Space temperature range	10~15	℃
HEX 6 efficiency	85	%
Pump isentropic efficiency	100	%
DHW		
Water Pressure	101.3	kPa
Inlet Temperature	25	℃
Outlet Temperature	60	℃

Energetic efficiency for each cycle is the ratio of power generation to heat addition, while overall power efficiency is the ratio of net power generated, to the fuel heating value required by the power plant. Furthermore, the overall efficiency of CCHP can be ascertained by the ratio of total products to the fuel consumed [20].

$$\eta_{th,cycle} = \frac{\dot{W}_{net,cycle}}{\dot{Q}_{in,cycle}} \quad (5)$$

$$\eta_{th,tot,Power} = \frac{\dot{W}_{net,tot}}{\dot{n}_f \overline{LHV}_f} \quad (6)$$

$$\eta_{th,tot,CCHP} = \frac{\dot{W}_{net,tot} + \dot{Q}_{Refrigeration} + \dot{Q}_{DHW} + \dot{Q}_{LNG}}{\dot{n}_f \overline{LHV}_f} \quad (7)$$

Where $\dot{Q}_{Refrigeration}$, $\dot{Q}_{DHW}$ and $\dot{Q}_{LNG}$ are the refrigeration capacity, heat demand for DHW and the required heat for LNG regasification before being distributed through natural gas pipelines, respectively. The chemical reaction in the CC can be represented by the following equation, which is contingent upon the fuel-to-air ratio [20].

$$\bar{\lambda}\,(CH_4) + [0.2059\,O_2 + 0.7748\,N_2 + 0.0003\,CO_2 + 0.019\,H_2O] \rightarrow (1+\bar{\lambda})\,[Y_{CO_2}CO_2 + Y_{H_2O}H_2O + Y_{O_2}O_2 + Y_{N_2}N_2] \quad (8)$$

Where $\bar{\lambda}$ is the ratio of fuel molar flow rate to air molar flow rate, as described in Equation (9).

$$\bar{\lambda} = \frac{\dot{n}_f}{\dot{n}_a} \quad (9)$$

The molar flow rate of the combustion products in the CC can be determined using $\bar{\lambda}$, as indicated in Equation (10).

$$\frac{\dot{n}_p}{\dot{n}_a} = 1 + \bar{\lambda} \quad (10)$$

Here $\dot{n}_p$ and $\dot{n}_a$ represent the molar flow rates of exhaust gases and air input, respectively. The mole fractions of the exhaust gases are derived using the following equations.

$$Y_{CO_2} = \frac{0.0003 + \bar{\lambda}}{1 + \bar{\lambda}} \quad (11)$$

$$Y_{H_2O} = \frac{0.019 + 2\,\bar{\lambda}}{1 + \bar{\lambda}} \quad (12)$$

$$Y_{O_2} = \frac{0.2059 - 2\,\bar{\lambda}}{1 + \bar{\lambda}} \quad (13)$$

$$Y_{N_2} = \frac{0.7748}{1 + \bar{\lambda}} \quad (14)$$

In the steady-state condition, the energy balance for the CC is represented by Equation (15).

$$\dot{Q}_{CC} + \dot{n}_f \bar{h}_f - \dot{n}_p \bar{h}_p + \dot{n}_a \bar{h}_a = 0 \quad (15)$$

This paragraph presents assumptions and equations for determining unknown variables in the refrigeration cycle, assuming steady-state operation and defining mass and refrigerant conservation at cycle components.

$$\sum(X \cdot \dot{m})_{\text{in}} = \sum(X \cdot \dot{m})_{\text{out}} \quad (16)$$

Where X_i denotes the mass fraction of the refrigerant in the working fluid at State "i". In all examined articles, jacket heat transfer at the solution heat exchanger, pump, throttle valves, and throughout the piping system was disregarded, and this assumption is maintained in the current analysis. The Enthalpy of LiBr/Water solution as function of temperature, pressure, and mixture composition:

$$h = h(TiPjX) \quad (17)$$

Where ṁ is the mass-flow rate (kg·s^{-1}), h is the specific enthalpy (kJ·kg^{-1}), ex is the specific exergy (kJ·kg^{-1}), and T_0, p_0 denote the environmental reference state.

The analytical correlations utilized in this study, as proposed by Sun [21] and Patek and Klomfar [22,23], have been effectively employed in several prior investigations [24–26]. It is also assumed that pressure losses in all components except for pump and throttle valves are negligible. For the present study, the following equations apply:

$$P_{28} = P_{29} = P_{30} = P_{31} = P_{34} = P_{35} \quad (18)$$

$$P_{27} = P_{32} = P_{33} = P_{36} \quad (19)$$

Here are some additional assumptions about the inlet and outlet of components:

- State 27: Saturated liquid solution
- State 30: Saturated vapor refrigerant
- State 31: Saturated liquid refrigerant
- State 33: Saturated vapor refrigerant
- State 34: Saturated liquid solution

This study examines an effortless concept with the weak solution released from the top of the generator, where the refrigerant leaves in the vapor phase. In this configuration, the temperature at State 30 correlates to the equilibrium temperature of the weak solution at the generator pressure.

$$T_{30} = T_{\text{sat}}(P_{29}, X_{29}) \quad (20)$$

This study derives Q_{GEN} from the cooling heat output of OBC compressors, with T_{34} given, hence determining the design and dimensions of the heat exchanger. This study delineates the condensation temperature T_{31}, which is determined by selecting the ambient temperature and designing a condenser accordingly.

The same is true for the absorber exit temperature T_{27}. Eventually, the efficiency of the solution heat exchanger is specified.

$$\eta_{\text{SHEX}} = \frac{h_{29} - h_{28}}{h_{34} - h_{28}} \quad (21)$$

A guide that provides more details on the numerical solution of this analysis is given in [5], which can be consulted for more information. Finally, energy conservation is employed once more to determine the heat transfer rates at the condenser, evaporator, and absorber, as well as the power necessary to operate the pump. The study concludes with the computation of the Coefficient of Performance (COP) of the machine, defined as the ratio of the desired output, which is the cooling effect produced, to the required input for the machine's operation:

$$\text{COP} = \frac{\dot{Q}_{\text{evap}}}{\dot{Q}_{\text{des}} + \dot{W}_{\text{pump}}} \quad (22)$$

2.4 Exergy analysis

Assuming negligible kinetic and potential exergy, the specific exergy generally entails the physical and chemical exergy. Exergy rate, physical exergy, and chemical exergy are defined as follows, respectively [3,4]:

$$ex = ex_{\text{ph}} + ex_{\text{ch}} \quad (23)$$

$$ex_{\text{ph}} = (h - h_0) - T_0(s - s_0) \quad (24)$$

$$e_{\text{ch}} = \frac{\sum x_i e_{\text{ch},i} R T_0 + x_i \ln \sum x_i}{M} \quad (25)$$

$$I = \sum \dot{m}_{\text{in}} e_{\text{in}} - \sum \dot{m}_{\text{out}} e_{\text{out}} - \sum \frac{\dot{Q}}{T_r} + \dot{W} \quad (26)$$

Where M, h, s, and xi are the molecular weight, specific enthalpy and entropy, and mole fraction of component i, respectively. The values of the specific standard chemical exergy ($ex_{ch,i}$) can be detected in Ref. [27,28].

The following formulas [29] determine the exergy destruction rate ($Ex_{D,i}$), exergy destruction fraction ($Ex_{ratio,D,i}$), and exergy efficiency of components ($ex_{,i}$), respect-ively:

$$\dot{E}_{x,\mathrm{Des},i} = \sum \dot{E}_{x,\mathrm{in},i} - \sum \dot{E}_{x,\mathrm{out},i} \quad (27)$$

$$\dot{E}_{x,\mathrm{Des,ratio},i} = \frac{\dot{E}_{x,\mathrm{Des},i}}{\sum \dot{E}_{x,\mathrm{Des},i}} \quad (28)$$

$$\eta_{x,i} = \frac{\dot{E}_{x,\mathrm{out},i}}{\dot{E}_{x,\mathrm{in},i}} \quad (29)$$

Thermal exergy is calculated as follows [20]:

$$\dot{E}_{x,Q} = \left(1 - \frac{T_0}{T}\right)\dot{Q}_h \quad (30)$$

3. RESULTS AND DISCUSSION

The analysis based on the parameters described in Table 2 reveals a comparison of results derived from the thermodynamic modelling of Power generation subsystems, as referenced in [8], which is detailed in Table 3.

The calculations indicate that the maximum relative error of the current modelling results compared to the reference results stands at 2.8%. This demonstrates a commendable level of accuracy in alignment with the foundational modelling presented in the base paper.

Table 3. Comparison of the power-generation results in the present work [8].

Parameter	Present work	Reference [8]	Percentage of error
$\dot{W}_{LNG}(kW)$	2467	2369	4.1 %
$\dot{W}_{CBC}(kW)$	28247	28597	1.2 %
$\dot{W}_{OBC}(kW)$	110259	113920	3.2 %
$\dot{W}_{tot}(kW)$	140973	144886	2.7 %

3.1 LiBr/Water Absorption refrigeration subsystems validation:

The analysis based on the parameters outlined in Table 2 demonstrates a comparison of the results obtained from the thermodynamic modelling of the LiBr/water absorption refrigeration subsystem, as referenced in [30], which is detailed in Table 4. The calculations indicate that the maximum relative error of the current modelling results compared to the reference results is at 0.32%.

This value indicates an excellent level of accuracy in alignment with the foundational modelling presented in the base paper.

Table 4. LiBr/H_2O ARC results vs. [30]

Parameter	Present work	Ref [30]	Percentage of error
$\dot{Q}_{Generator}(kW)$	20	20	0%
$\dot{Q}_{Condenser}(kW)$	15.45	15.50	0.32 %
$\dot{Q}_{Evaporator}(kW$	14.84	14.87	0.20 %
$\dot{Q}_{Absorber}(kW)$	19.39	19.38	0.05 %
COP	0.742	0.743	0.13 %

3.2 Thermo-Exergy analysis of LNG-Coupled CCHP system

A crucial innovation entails the preheating of combustion fuel using exhaust gases, thus increasing the temperature and pressure of the fuel before its introduction into the CC. This method reduces fuel consumption and produces additional energy via the expansion of heated fuel within the turbine.

Moreover, the use of LNG-derived methane, rather than environmentally obtained methane, significantly improves efficiency due to its higher beginning pressure.

Table 5 delineates the thermodynamic parameters, including temperature, pressure, enthalpy, entropy, and total exergy for each condition.

Table 6 delineates the results and achievements of the proposed system, revealing a total net output power of 168.8 MW, alongside a cooling capacity of 11.7 MW and a hot water flow rate of 143.7 kg/s. The energy and exergy efficiencies of this system are 93.2% and 51%, respectively. The computation of first-law efficiency considers the energy absorbed in the LNG a notable achievement. The total exergy destruction is 137.2 MW, with the CC of the OBC subsystem contributing the most at 94.3 MW.

Table 5. Thermodynamic properties for states in the current work.

State -	Pressure (kPa)	Temperature (°C)	Enthalpy (kj/kg)	Entropy (kj/kg/K)	MM_i (kg/kmol)	$\dot{m}$ (kg/s)	$\dot{Ex}_{tot}$ (kW)
0	101.3	20	-	-	-	-	-
1	1000	-160	-904.5	-6.638	16.04	65.03	3.44×10^6
2	27200	-143.8	-810.9	-5.872	16.04	65.03	3.43×10^6
3	27200	87.3	-2.074	-2.798	16.04	65.03	3.42×10^6
4	8000	2	-148.4	-2.702	16.04	65.03	3.41×10^6
5	285	-128.8	-159.6	5.775	28.01	218.6	38723
6	4275	69.5	46.19	5.869	28.01	218.6	77670
7	4061	416.3	415.1	6.626	28.01	218.6	109815

8	300	103	81.01	6.755	28.01	218.6	28530
9	101.3	20	-169.6	6.937	28.65	202.4	687.5
10	656.5	245.2	63.23	6.983	28.65	202.4	45084
11	643.4	104.5	-83.2	6.659	28.65	202.4	34645
12	636.9	35	-154.3	6.454	28.65	202.4	32424
13	4255	275.6	95.35	6.501	28.65	202.4	80190
14	4106	1290	-54.02	7.998	28.07	207.8	271072
15	103.4	436.3	-1133	8.099	28.07	207.8	40572
16	101.3	89.5	-1521	7.357	28.07	207.8	5117
17	101.3	85.2	-1526	7.345	28.07	207.8	4937
18	8000	2	-148.4	-2.702	16.04	5.437	285365
State	**Pressure**	**Temperature**	**Enthalpy**	**Entropy**	$\boldsymbol{MM_i}$	$\dot{\boldsymbol{m}}$	$\boldsymbol{\dot{Ex}_{tot}}$
-	(kPa)	(℃)	(kj/kg)	(kj/kg/K)	(kg/kmol)	(kg/s)	(kW)
19	8000	79.5	-4523	9.734	16.04	5.437	285539
20	4297	41	-4614	9.785	16.04	5.437	284967
21	7.907	40	-132.331	-0.37986	92.14	54.2	58876
22	276	40.1	-131.973	-0.37975	92.14	54.2	58894
23	276	150	414.8687	0.989147	92.14	54.2	66782
24	7.907	71.7	311.374	1.030714	92.14	54.2	60512
25	111.4	20	84.02	0.2965	18.02	143.8	7185
26	111.4	60	251.3	0.8312	18.02	143.8	8690
27	0.8725	30	69.26	0.205	30.86	19.12	11480
28	4.247	30	69.26	0.205	30.86	19.12	11480
29	4.247	64.6	142.6	0.434	30.86	19.12	11599
30	4.247	57.9	2609	8.619	18.02	4.914	661.8
31	4.247	30	125.7	0.4368	18.02	4.914	248.4
32	0.8725	5	125.7	0.4527	18.02	4.914	225.4
33	0.8725	5	2510	9.025	18.02	4.914	-406.4
34	4.247	100	302.4	0.505	40.98	14.2	13486
35	4.247	40.6	203.8	0.217	40.98	14.2	13283
36	0.8725	40.6	203.8	0.217	40.98	14.2	13283
37	101.3	15	63.08	0.2244	18.02	559	28030
38	101.3	10	42.12	0.1511	18.02	559	28338

Table 6. Proposed CCHP's key results.

Power	**Value**	$\boldsymbol{\eta_I}$ **(%)**	$\boldsymbol{\eta_{II}}$ **(%)**
$\dot{W}_{LNG}$	5.8 *(MW)*	10.6	-
$\dot{W}_{CBC}$	30.8 *(MW)*	34.3	-
$\dot{W}_{OBC}$	126.6 *(MW)*	46.5	-
$\dot{W}_{ORC}$	5.6 *(MW)*	18.9	-
$\dot{W}_{tot}$	168.8 *(MW)*	62	58.7
$\dot{Q}_{Ref}$	11.7 *(MW)*	-	-
$\dot{Q}_{DHW}$	24 *(MW)*	-	-
$\dot{m}_{DHW}$	143.7 *(kg/s)* @ 60℃	-	-
$\dot{Q}_{HLNG}$	54.5 *(MW)*	-	-

3.3 Effect of CC Temperature on the system power generation rate

Figure 2 illustrates the impact of CC temperature on the net power production of the subsystems over various system cycles. The total net power output exhibits an upward trend with rising temperature; however, beyond approximately 1250 °C, this trend turns to a gradual decrease. This change is attributed to the dominance of the decreasing effects on power production from the three cycles: OBC, ORC, and LNG, which exceed the increasing trend in the work produced by the CBC. The net power of the CBC initially exhibits a slight increase attributed to the rise in enthalpy to entry into the gas turbine, subsequently entering an endured reduction. This trend is primarily due to the accelerated decrease in the airflow rate, which exceeds the gradual increase in CC temperature.

The dropped airflow rate is made worse by the raised equivalence ratio necessitated by the demand for higher temperatures within the CC.

Because of the reduced airflow rate in the OBC, the thermal heat source to the ORC, LiBr/Water, and LNG cycles must be notably restricted, leading to a corresponding reduction in their net power generation.

In contrast, the net power of the CBC, which is dependent on the high-temperature source (gas turbine output) and the constant low-temperature source (LNG cycle), demonstrates an excellent upward path with rising gas turbine output temperature, initially at a steep slope and subsequently at a more gradual rate.

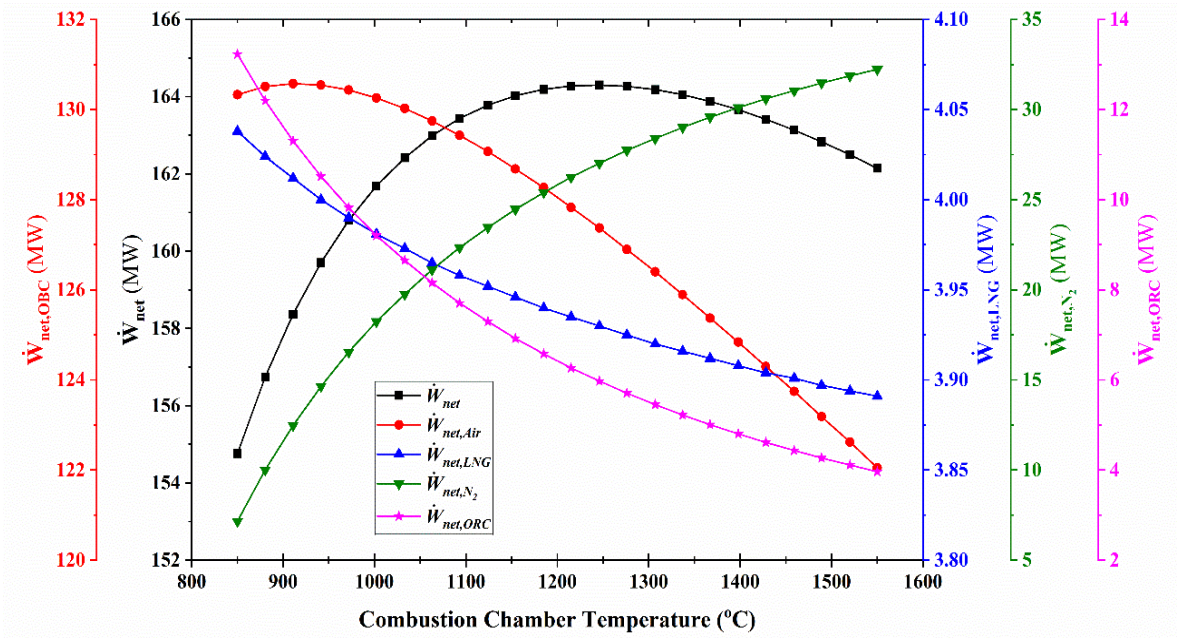

Figure 2. Evaluation of Produced Works versus CC temperature.

3.4 Effect of CC Temperature on the system overall production

Figure 3 illustrates the impact of CC temperature on the system overall production. The total net power output exhibits an upward trend with rising temperature; however, then this trend turns to a gradual decrease as described in previous section.

The overall amount of domestic hot water supplied, as well as the cooling capacity due to the reduction in airflow rate within the OBC, decreases as the CC temperature rises. Conversely, the rise in CC temperature and corresponding increase in the equivalency ratio result from a raised fuel-to-air ratio and a reduced airflow rate. Nevertheless, as the fuel flow rate has decreased in correlation with the reduction in airflow, the denominator of Equation (6) decreases according to the efficiency relationship.

At the same time, the total useful work produced at various temperatures exhibits either a steady rise or a slight decreasing trend; thereby, the first-law efficiency of the cycle consistently rises. Within the efficiency range associated with combined cooling, heat, and power (CCHP), earlier trends and reasons persist, leading to a continuous increase in the first-law efficiency of CCHP.

3.5 Effect of CC Temperature on the system overall performances:

Figure 4 shows the effect of increasing the temperature of the OBC - CC on the first and second law efficiencies from the perspective of power production and also from the perspective of combined cooling, heat and power (CCHP) production.

The first and second law efficiencies from the perspective of system power production have been explained in the previous section, the first and second law efficiencies from the perspective of combined cooling, heat and power (CCHP) production are explained in this section, the four efficiencies are always increasing due to the increase in the temperature of the CC, the reason for this increasing trend was explained in the previous section, but the point to note in this plot is that, as we expect, the first law efficiency from the perspective of combined production is greater than the first law efficiency from the perspective of power production, which is due to the use of waste heat from the power production section to produce heat and cooling in different sections of the system. But on the other hand, the second law efficiency from the perspective of the combined cycle is, contrary to expectations, lower than the second law efficiency from the perspective of power.

The reason for this behaviour can be explained as follows: in the previous sections (including the first law efficiency), we considered LNG heating as part of our products and demands, which has increased the efficiency from the first law perspective. However, from the second law perspective, the exergy of cold LNG is much higher than the exergy of methane gas close to ambient temperature. Therefore, if we repeat the same approach as we considered in the first law, the exergy changes in LNG regasification process have a negative effect on the exergy efficiency (second law efficiency), which has caused it to decrease and place it at the lowest position in the graph.

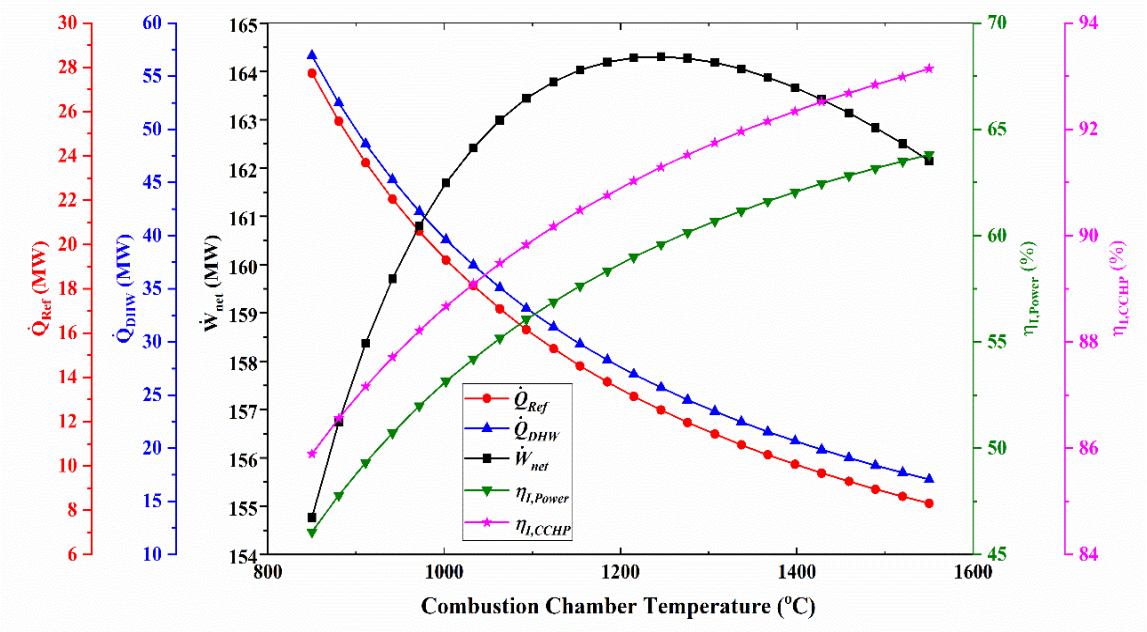

Figure 3. Assessment of CCHP parameters in relation to CC temperature

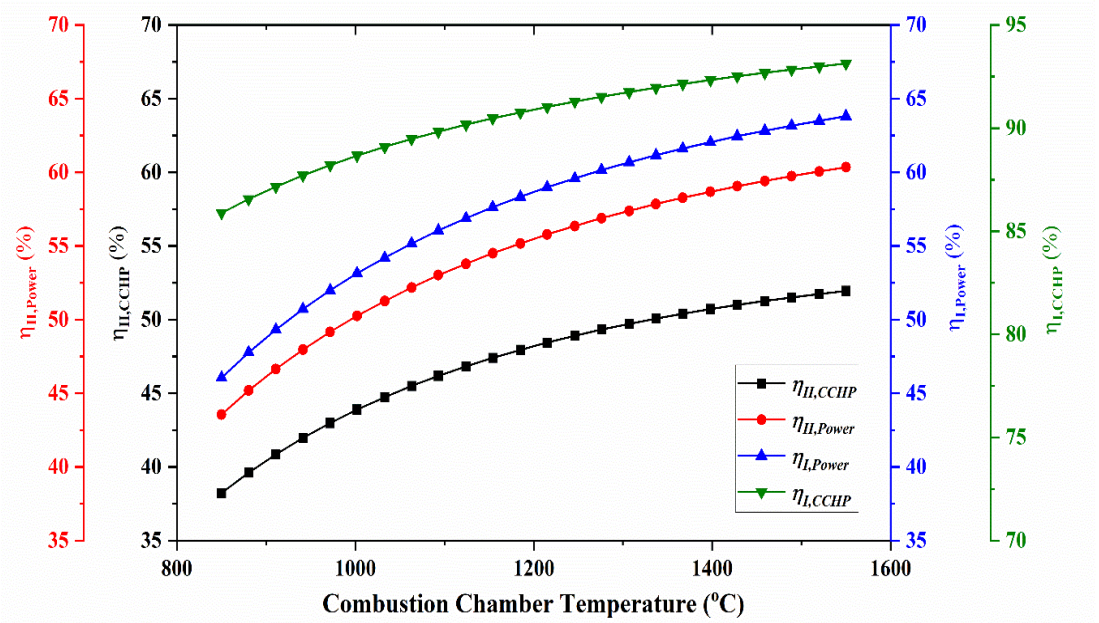

Figure 4. Assessment of performance of overall systems in relation to CC temperature.

3.6 Effect of Compressor Pressure Ratio on the system power generation rate:

Figure 5 shows the effect of compressor pressure ratio (PRC) on the net power production of subsystems in different cycles of the system. The total net power produced shows an upward trend with increasing pressure ratio, which indicates that the trend of increasing power production in OBC and ORC prevails over the downward trend of power production in CBC (N2 Cycle) and LNG systems. With increasing pressure ratio, first the temperature range between the compressors of the OBC system increases, as a result, the heat source temperature for ORC systems, domestic hot water (DHW), and LiBr/Water absorption refrigeration systems will also increase, which will result in an increase in the production of these systems.

On the other hand, with increasing pressure ratio, the gas turbine outlet flow temperature decreases significantly, which will result in a decrease in the source temperature for the CBC system and the second turbine of the LNG system, which naturally affects and reduces the production of these two systems, but the intensity of this decrease is always less than the intensity of the increase in the production of other sections of the overall system, as a result , the overall trend of power production in the system is always increasing.

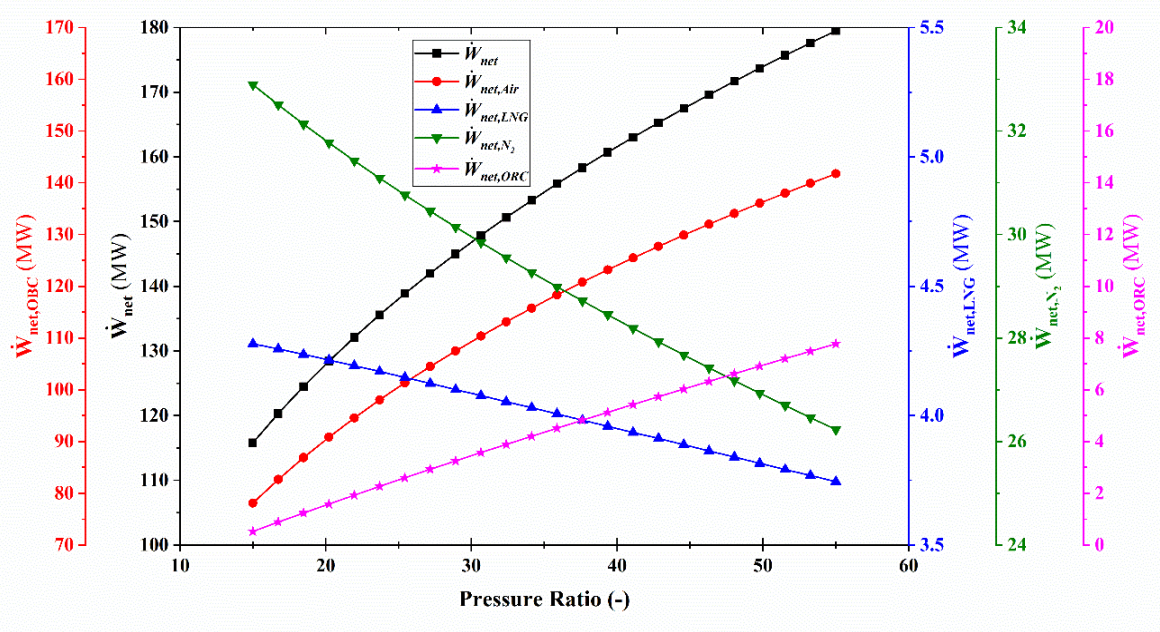

Figure 5. Evaluation of Produced Works versus Compressor pressure ratio in CBC subsystem

3.7 Effect of Compressor Pressure Ratio on the system overall production:

Figure 6 shows the effect of compressor pressure ratio on the total system output, including heat, cooling, and power. The total net power generation increases with increasing pressure ratio. The total amount of domestic hot water supplied also increases due to the increase in heat input to the ORC system, but this increase in heat input to the ORC section and the presence of a pinch point setting in its corresponding heat exchanger causes the outlet flow temperature decrease of heat exchanger of the OBC system significantly with increasing pressure ratio, which results in a decrease in the inlet temperature to the LiBr/Water absorption refrigeration cycle generator and, as a result, a slight decrease in cooling output (due to the increase in air flow rate, there is a positive effect to compensate for this decrease).

The overall system efficiency, from the perspective of the first law and power generation, exhibits a nearly constant trend, while the overall efficiency of the CCHP system also demonstrates a similar trend but is positioned at a higher level.

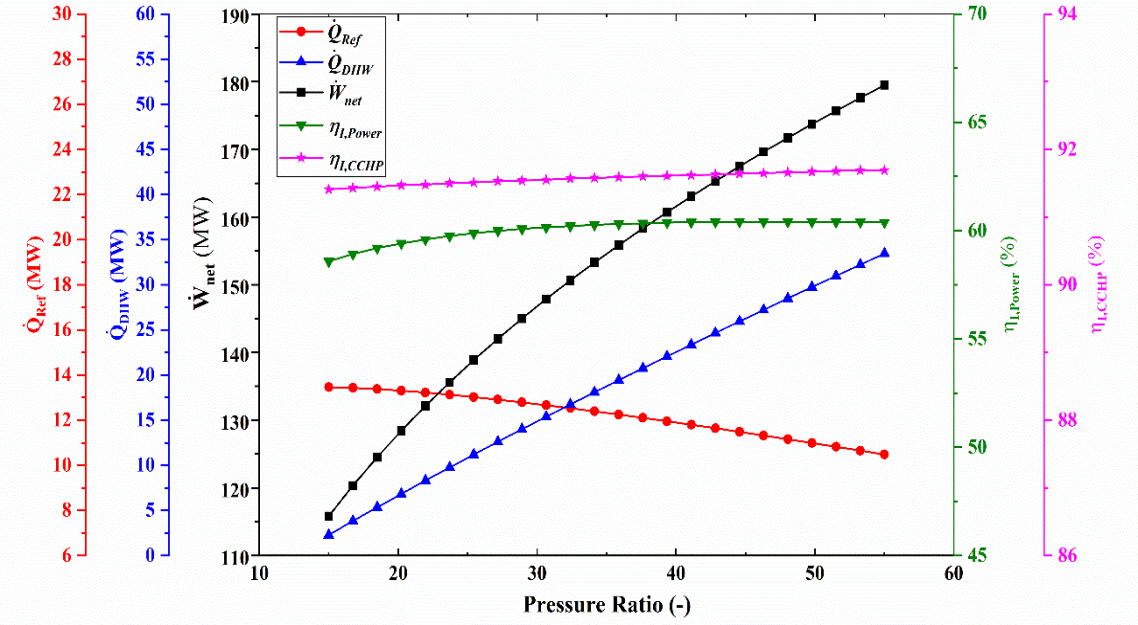

Figure 6. Evaluation of compressor pressure ratio on the system overall production.

3.8 Effect of Compressor Pressure Ratio on the system overall performances

Figure 7 illustrates the impact of variations in the compressor pressure ratio inside the OBC subsystem on both the first and second law efficiencies, including power generation as well as CCHP output. The efficiency of the first and second laws of system power production have been elucidated in the preceding section.

As illustrated in the picture, all four efficiencies consistently exhibit a minor increase attributable to the rise in the PRC. The first law efficiency from the standpoint of combined production exceeds that of power production, as anticipated; this disparity results from the utilization of waste heat from the power production segment to facilitate heating and cooling in different sections of the system, as previously indicated. Conversely, the second law efficiency from the standpoint of the combined cycle is, contrary to expectations, inferior to the second law efficiency from the perspective of power.

This behaviour can be elucidated as follows: In the preceding sections, including the discourse on first law efficiency, we considered LNG heating as integral to our products and demands, resulting in an enhancement in efficiency from the first law standpoint.

From a second-law standpoint, the exergy of cold LNG significantly exceeds that of methane gas at ambient temperatures. Consequently, if we replicate the methodology employed in the first law, the exergy alterations in the LNG regasification process adversely impact the exergy efficiency (second law efficiency), resulting in a decline and positioning it at the lowest point on the graph.

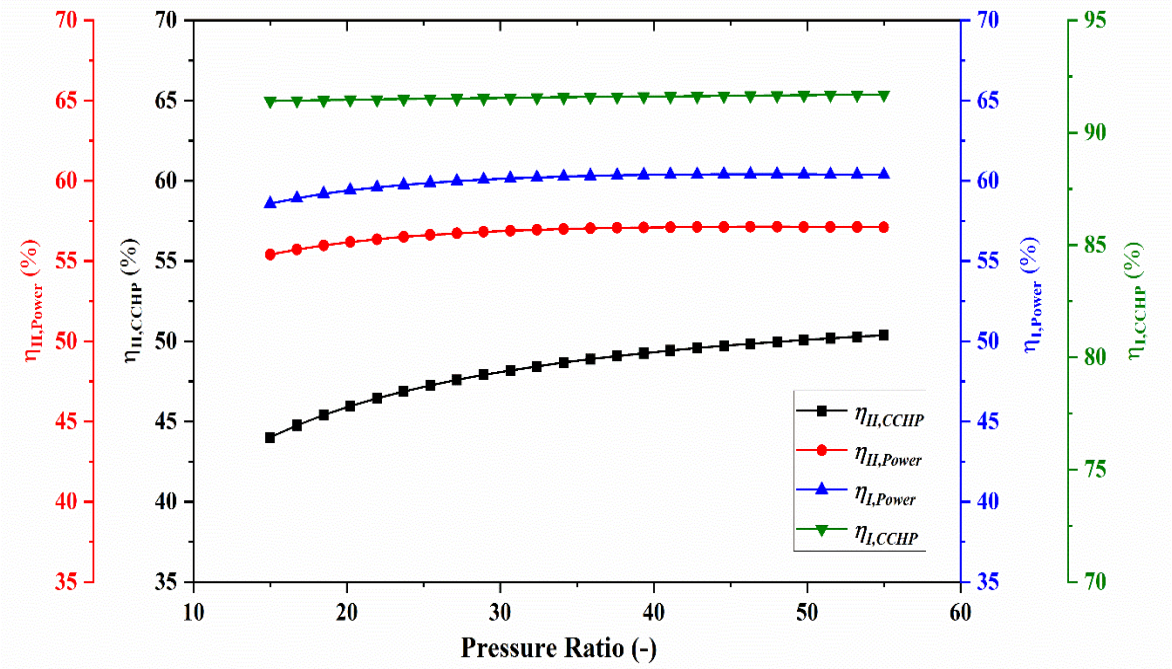

Figure 7. Evaluation of Compressor Pressure Ratio on the system overall performances.

3.9 Effect of LNG Pump Ratio on the system power generation

Figure 8 shows the effect of the pressure ratio of the LNG regasification system (LNGP) pump on the net power generation of the subsystems in the entire system. The total net power generated shows an upward trend with increasing pressure ratio, which indicates that the trend of increasing power generation in the OBC, ORC and LNG systems dominates the overall downward trend of power generation in the CBC system (N2 cycle). With increasing pressure ratio, the outlet temperature of the LNG system pump increases, as a result, the temperature of the CBC cycle heat well increases, which causes a decrease in cycle performance.

However, on the other hand, this increase in pressure ratio causes an increase in the flow rate of the different cycles in the entire subsystems, which causes an increase in the power generation in most of them, but as can be seen, the effect of changes in this parameter, i.e. the pressure ratio of the LNG regasification system pump, is not so noticeable compared to the other parameters under study.

3.10 Effect of LNG Pump Ratio on the system overall production

Figure 9 shows the effects of changing the pump pressure ratio of the LNG regasification system on the total useful output of the system, including heat, cooling, and electrical power generation. The total net power generation always increases with increasing pressure ratio, as discussed in the previous section. As mentioned earlier, with increasing this pressure ratio, the flow rate of the subsystem fluids increases, resulting in an increase in the total amount of domestic hot water supplied due to the increase in heat input to the ORC system and the refrigeration capacity created in the absorption refrigeration subsystem. The overall efficiency of the system, from the perspective of the first law and electricity generation, shows an almost decreasing trend, as does the overall efficiency of the CCHP system, which also shows a similar trend but at a higher level.

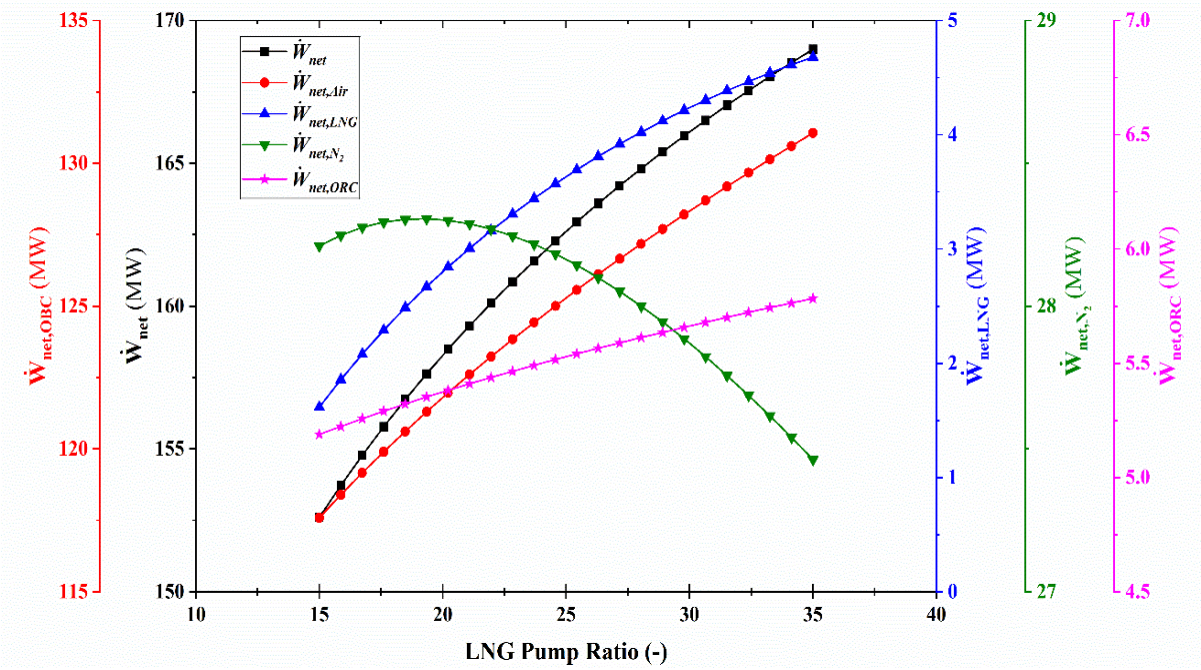

Figure 8. Assessment of the Impact of LNG Pump Ratio on System Power Generation

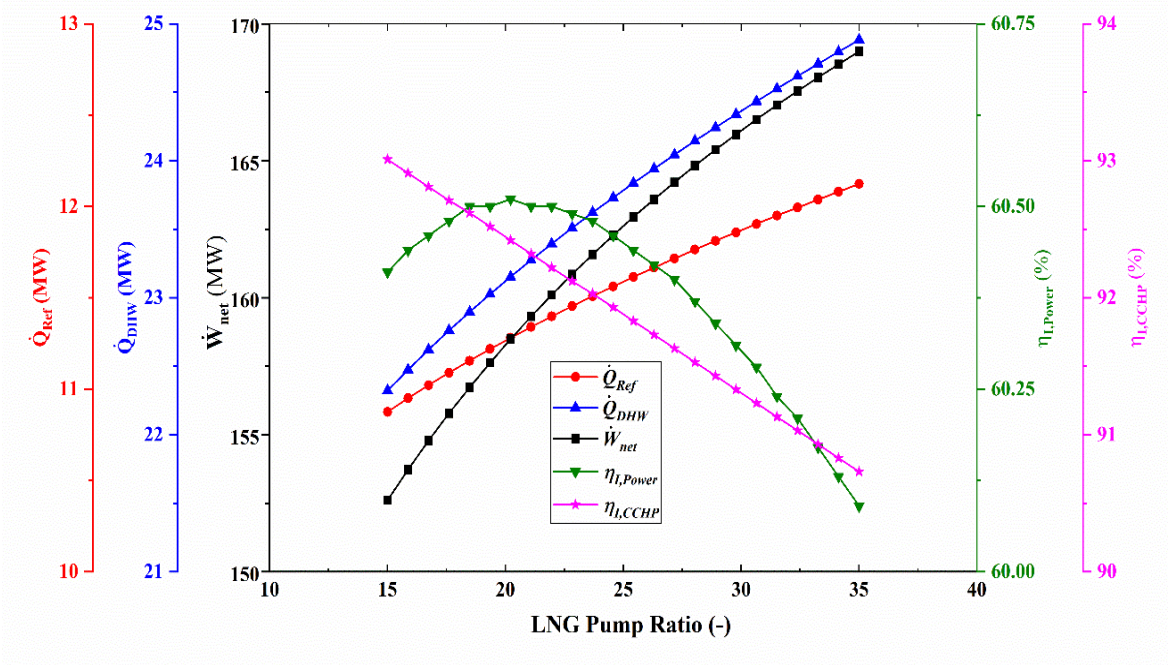

Figure 9. Assessment of the Impact of LNG Pump Ratio on the overall production

3.11 *Effect of LNG Pump Ratio on the system overall performances*

Figure 10 examines the changes in the first and second law efficiencies of the recommended system due to changes in the pump pressure ratio of the LNG subsystem. The first and second law efficiencies of the total system net power generation were generally explained in the previous section. All four efficiencies follow a nearly constant trend.

The first law efficiency from the combined generation perspective is, as expected, higher than the power generation efficiency. This difference is due to the use of waste heat from the power generation section to facilitate heating and cooling in different parts of the system, but this efficiency is always decreasing with increasing pump pressure ratio. The reason for this performance decreases is the slower growth of energy recovery from waste heat in different parts compared to the higher growth of fuel consumption with increasing pump pressure ratio.

As reiterated in the previous sections, the second law efficiency of combined generation is lower than the second law efficiency of power generation alone. This behaviour can be explained as follows: In the previous sections, including the discussion of the first-law efficiency, LNG heating adversely affects the exergy efficiency (second-law efficiency), leading to its decrease and placement at the lowest point of the graph.

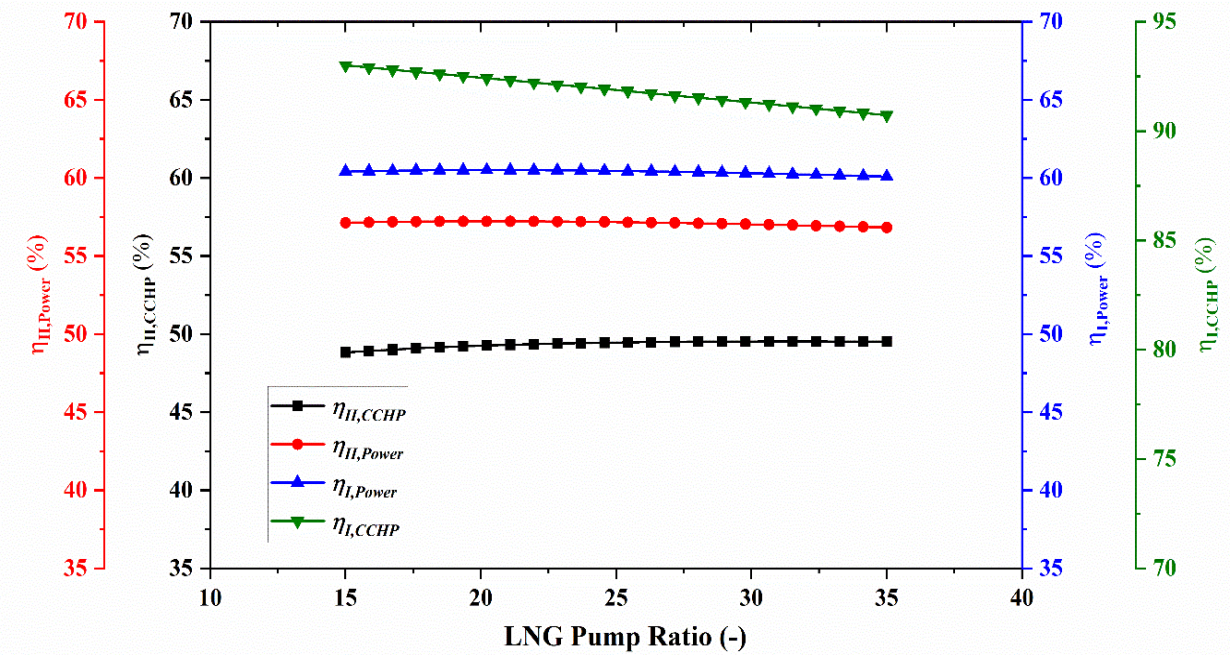

Figure 10. Assessment of the impact of LNG pump pressure ratio on overall performances for power-only and CCHP bases.

4. CONCLUSION:

The study set out to demonstrate how the cryogenic exergy released during LNG regasification can be channelled through a tightly coupled CCHP facility rather than being dissipated to seawater. A full-plant model, implemented and validated in Engineering Equation Solver, linked a closed Brayton cold-box, a conventional gas-turbine combined cycle and a lithium-bromide/water absorption refrigeration loop with the LNG send-out line.

Solving mass, energy and exergy balances for each component enabled an internally consistent appraisal of power-only, CHP and CCHP operating modes across a 160 MW-class plant and permitted systematic exploration of combustor outlet temperature, compressor pressure ratio, regasification pressure and heat-exchanger pinch point. Four principal insights emerge:

- Exergy accounting shows that seventy per cent of the total irreversibility concentrates in the CC, with the share split almost evenly between chemical and thermal losses. This localisation means that incremental improvements in flame management or staged combustion yield disproportionately large system-wide benefits.
- An optimum regasification-pressure window of 6–7 MPa maximises the trade-off between LNG pump work, valve throttling losses and useful cold-energy recovery; moving outside this window erodes overall exergy efficiency by up to three percentage points.
- The closed Brayton cold-box converts seventy-eight per cent of the incoming cryogenic exergy into either chilled water or feed-water heating,

proving that deep refrigeration stages are unnecessary.

- Integrating all three sub-cycles lifts overall exergy efficiency from 41 % in the best reference layout to 51 % here and cuts specific fuel consumption by approximately one fifth at identical net power output.

Concentration of exergy destruction in the combustor justifies prioritising lean-premixed or sequential burners, exhaust-gas recirculation and advanced coatings that limit flame temperature without sacrificing turbine inlet conditions. The identified regasification-pressure window offers a concrete specification for LNG terminal pumps and pipelines, easing coordination between power-plant operators and mid-stream gas suppliers. Heat-exchanger analysis supports adopting printed-circuit or spiral-wound units with pinch points no tighter than 5 K, balancing capital cost against incremental thermodynamic returns.

Several limitations should be acknowledged. The calculations were carried out under steady-state, full-load conditions; dynamic behaviour during start-up, shutdown and load-following, particularly the interaction of the absorption chiller with variable cooling demand, remains unexplored. The analysis focused on thermodynamic performance; levelised cost of energy, life-cycle greenhouse-gas emissions and operability in real-world ambient conditions were not quantified. Mechanical fatigue in printed-circuit heat exchangers subjected to repeated cryogenic cycling and potential icing in the LNG throttle valve were outside the present scope. These caveats mean that the numerical gains reported here should be interpreted as an upper bound until validated by experimental data.

NOMENCLATURE

Acronyms	
ARC	Absorption Refrigeration Cycle
CBC	Closed Brayton Cycle
CC	Combustion chamber
CCHP	Combined Cooling, Heat and Power
CETD	Corrected End Temperature Difference
DHW	Domestic Hot Water
EES	Engineering Equation Solver
HEX	Heat Exchanger
LNG	Liquefied Natural Gas
OBC	Open Brayton Cycle
ORC	Organic Rankine cycle
$T_{C.C.}$	Combustion Chamber Temperature
Latin symbols	
$\dot{Q}$	Heat transfer rate
$\dot{m}$	Mass flow rate
$\dot{n}$	Molar flow rate
$\dot{W}$	Produced/consumed power
cp(T)	Temperature-dependent specific heat at constant pressure
h	Specific enthalpy
LHV	Lower heating value
P	Pressure
s	Specific entropy
T	Temperature
y	Mole fraction
Subscripts	
0	Restricted dead state
a	Air
cv	Control volume
f	Fuel
i	Inlet
p	Products
ref	Reference (where used)
th	Thermo-mechanical
tot	Total
e	Exit
Greek letters	
η	Efficiency
φ	Equivalence ratio (fuel–air equivalence)
$\bar{\lambda}$	Fuel flow rate to air flow rate

REFERENCES

[1] Javaherian A, Ghasemi S, Seyed Mahmoudi SM, Rosen MA, Sadeghi M. Two-Objective Optimization of a Cogeneration System Based on a Gas Turbine Integrated with Solar-Assisted Rankine and Absorption Refrigeration Cycles. Sustainability 2023;15. https://doi.org/10.3390/su152115624.

[2] Zeinali M, Sharifi A, Ranjbar F. Thermodynamic analysis of sustainable electric power production using solar tower during day and syngas combustion from municipal waste gasification during night. Energy Equip Syst 2023;11:277–304. https://doi.org/10.22059/ees.2023.1999210.1421.

[3] Sharafi laleh S, Zeinali M, Mahmoudi SMS, Soltani S, Rosen MA. Biomass co-fired combined cycle with hydrogen production via proton exchange membrane electrolysis and waste heat recovery: Thermodynamic assessment. Int J Hydrogen Energy 2023;48:33795–809. https://doi.org/https://doi.org/10.1016/j.ijhydene.2023.05.137.

[4] Ghiami Sardroud R, Javaherian A, Seyed Mahmoudi SM, Akbari Kordlar M, Rosen MA. Proposal and Comprehensive Analysis of a Novel Combined Plant with Gas Turbine and Organic Flash Cycles: An Application of Multi-Objective Optimization. Sustainability 2023;15. https://doi.org/10.3390/su151914152.

[5] Cao Y, Dhahad HA, Togun H, Anqi AE, Farouk N, Farhang B. Proposal and thermo-economic optimization of using LNG cold exergy for compressor inlet cooling in an integrated biomass fueled triple combined power cycle. Int J Hydrogen Energy 2021;46:15351–66. https://doi.org/10.1016/j.ijhydene.2021.02.111.

[6] Khanmohammadi S, Soyturk G, Kizilkan O. Thermal performance evaluation and multi-objective optimization of a hybrid system integrating biogas gas turbine, CO2 cycles, cold energy recovery, cooling and hydrogen production. Int J Hydrogen Energy 2025. https://doi.org/https://doi.org/10.1016/j.ijhydene.2025.03.224.

[7] Yousef MS, Hawwash AA, Santana D. Assessment of a sustainable multigeneration system integrating supercritical

CO2 Brayton cycle and LNG regasification: Thermodynamic and exergoeconomic evaluation. Case Stud Therm Eng 2024;56:104205. https://doi.org/https://doi.org/10.1016/j.csite.2024.104205.

[8] Tsatsaronis G, Morosuk T. Advanced exergetic analysis of a novel system for generating electricity and vaporizing liquefied natural gas. Energy 2010;35:820–9. https://doi.org/10.1016/j.energy.2009.08.019.

[9] Yehia F, Al-Haimi AANM, Byun Y, Kim J, Yun Y, Lee G, et al. Integration of the single-effect mixed refrigerant cycle with liquified air energy storage and cold energy of LNG regasification: Energy, exergy, and efficiency prospectives. Energy 2024;306:132567. https://doi.org/https://doi.org/10.1016/j.energy.2024.132567.

[10] Xu Z, Huang J, Muhammad T, Agrawal MK, Ayadi M, Ahmed MA, et al. Design and comprehensive thermo-enviro-economic assessment of an innovative polygeneration system using biomass fuel and LNG regasification: A CCHP-thermally desalination application. Process Saf Environ Prot 2024;183:925–44. https://doi.org/https://doi.org/10.1016/j.psep.2024.01.040.

[11] Zhao T, Ahmad SF, Agrawal MK, Ahmad Bani Ahmad AY, Ghfar AA, Valsalan P, et al. Design and thermo-enviro-economic analyses of a novel thermal design process for a CCHP-desalination application using LNG regasification integrated with a gas turbine power plant. Energy 2024;295:131003. https://doi.org/https://doi.org/10.1016/j.energy.2024.131003.

[12] Liu M, Lior N, Zhang N, Han W. Thermoeconomic analysis of a novel zero-CO2-emission high-efficiency power cycle using LNG coldness. Energy Convers Manag 2009;50:2768–81. https://doi.org/10.1016/j.enconman.2009.06.033.

[13] Liang P, Guo Y, Chauhdary ST, Agrawal MK, Ahmad SF, Bani Ahmad AYA, et al. Sustainable development and multi-aspect analysis of a novel polygeneration system using biogas upgrading and LNG regasification processes, producing power, heating, fresh water and liquid CO2. Process Saf Environ Prot 2024;183:417–36. https://doi.org/https://doi.org/10.1016/j.psep.2024.01.003.

[14] Salehi S, Javanfam F. Investigation of a novel solar-assisted multigeneration system comprising water desalination systems, an absorption refrigeration system, a single-effect absorption heat transformer and two organic Rankine cycles. Heliyon 2024;10. https://doi.org/10.1016/j.heliyon.2024.e36452.

[15] Emadi MA, Mahmoudimehr J. Modeling and thermo-economic optimization of a new multi-generation system with geothermal heat source and LNG heat sink. Energy Convers Manag 2019;189:153–66. https://doi.org/https://doi.org/10.1016/j.enconman.2019.03.086.

[16] Taheri MH, Mosaffa AH, Farshi LG. Energy, exergy and economic assessments of a novel integrated biomass based multigeneration energy system with hydrogen production and LNG regasification cycle. Energy 2017;125:162–77. https://doi.org/https://doi.org/10.1016/j.energy.2017.02.124

[17] Hu Y, Badrawi SI, Kumar J, Sabeh HN, Alsenani TR, Riaz F, et al. Gas turbine-based system taking advantage of LNG regasification process for multigeneration purposes; Techno-economic-environmental analysis and machine learning optimization. Process Saf Environ Prot 2023;179:10–26. https://doi.org/https://doi.org/10.1016/j.psep.2023.08.068.

[18] Hamada KI, Mohammed MN, Jasim RR, Ibrahim TK. Energy and exergy analyses of a combined power plant based on natural gas combustion. Tikrit J Eng Sci 2023;30(3):17–26. https://doi.org/10.25130/tjes.30.3.3

[19] Mohammed MK, Al Doori WH, Jassim AH, Ibrahim TK, Al-Sammarraie AT. Energy and exergy analysis of the steam power plant based on effect the numbers of feed water heater. J Adv Res Fluid Mech Therm Sci 2019;56(2):211–222.

[20] Moran MJ, Shapiro HN, Boettner DD, Bailey MB. Fundamentals of Engineering Thermodynamics, 9th Edition EPUB Reg Card Loose-Leaf Print Companion Set. Wiley; 2018.

[21] Xia G, Sun Q, Cao X, Wang J, Yu Y, Wang L. Thermodynamic analysis and optimization of a solar-powered transcritical CO2 (carbon dioxide) power cycle for reverse osmosis desalination based on the recovery of cryogenic energy of LNG (liquefied natural gas). Energy 2014;66:643–53. https://doi.org/10.1016/j.energy.2013.12.029.

[22] Pátek J, Klomfar J. A computationally effective formulation of the thermodynamic properties of LiBr–H2O solutions from 273 to 500 K over full composition range. Int J Refrig 2006;29:566–78.

[23] Pátek J, Klomfar J. A simple formulation for thermodynamic properties of steam from 273 to 523 K, explicit in temperature and pressure. Int J Refrig 2009;32:1123–5.

[24] Şencan A, Yakut KA, Kalogirou SA. Exergy analysis of lithium bromide/water absorption systems. Renew Energy 2005;30:645–57.

[25] Gomri R. Second law comparison of single effect and double effect vapour absorption refrigeration systems. Energy Convers Manag 2009;50:1279–87.

[26] Yan X, Chen G, Hong D, Lin S, Tang L. A novel absorption refrigeration cycle for heat sources with large temperature change. Appl Therm Eng 2013;52:179–86.

[27] Rujing Y, Wang J, Cheng Y, Ma C, Yu T. Thermodynamic analysis of fuel cell combined cooling heating and power system integrated with solar reforming of natural gas. Sol Energy 2020;206:396–412. https://doi.org/10.1016/j.solener.2020.05.085.

[28] Palacios-Bereche R, Gonzales R, Nebra SA. Exergy calculation of lithium bromide–water solution and its application in the exergetic evaluation of absorption refrigeration systems LiBr-H2O. Int J Energy Res 2012;36:166–81. https://doi.org/https://doi.org/10.1002/er.1790.

[29] Wu Z, Zhu P, Yao J, Zhang S, Ren J, Yang F, et al. Combined biomass gasification, SOFC, IC engine, and waste heat recovery system for power and heat generation: Energy, exergy, exergoeconomic, environmental (4E) evaluations. Appl Energy 2020;279:115794. https://doi.org/10.1016/j.apenergy.2020.115794.

[30] Wonchala J, Hazledine M, Goni Boulama K. Solution procedure and performance evaluation for a water–LiBr absorption refrigeration machine. Energy 2014;65:272–84. https://doi.org/https://doi.org/10.1016/j.energy.2013.11.087.